Science of the Total Environment 783 (2021) 147005

Contents lists available at ScienceDirect

Science of the Total Environment

journal homepage: www.elsevier.com/locate/scitotenv

Analysis of soil color variables and their relationships between two field-based methods and its potential application for wetland soils

Stephanie A. Schmidt, Changwoo Ahn *

Environmental Science and Policy, George Mason University, 4400 University Drive, MS5F2, Fairfax, VA 22030-444, United States of America

HIGHLIGHTS

- The Nix Color Sensor (NCS) can identify soil colors using variables beyond hue, value, and chroma of the Munsell system.
- NCS variables could modestly (hue) or moderately strongly (value, chroma) predict Munsell Soil Color Chart (MSCC) variables.
- Further study of the NCS is needed to discern its usefulness in assessing wetland soil colors and delineating hydric soils.

GRAPHICAL ABSTRACT

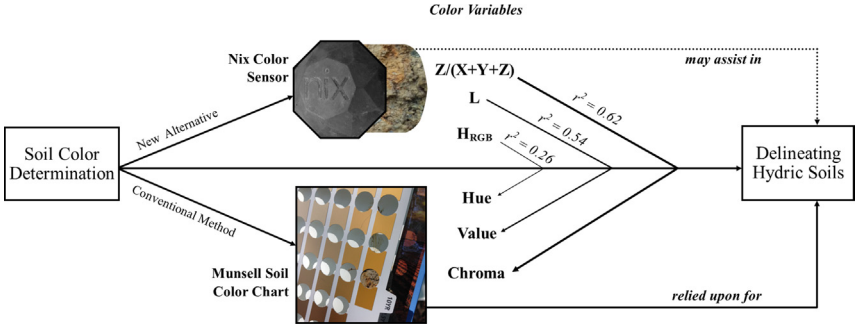

ARTICLE INFO

Article history:
Received 28 November 2020
Received in revised form 13 March 2021
Accepted 2 April 2021
Available online 10 April 2021

Editor: Jan Vymazal

Keywords:
Soil color
Hydric soils
Wetland soil
Munsell Soil Color Chart
Nix Color Sensor
Wetland delineation

ABSTRACT

While the Munsell Soil Color Chart (MSCC) is the most frequently used, well-established field method for reading soil color, the Nix Color Sensor (NCS) is an inexpensive, app-based alternative that can complement or potentially substitute for the MSCC. Soils were collected and their colors were measured from four forested sites across Northern Virginia within the Chesapeake Bay Watershed using both the MSCC and NCS. Three MSCC variables and 15 NCS variables were collected in the field; a methodology was established to use these "measured" (M) variables to derive 9 NCS calculated (C) variables. A stepwise correlation identified NCS variables most suitable for relating the NCS to each of the MSCC attributes: hue (H), value (V), and chroma (C_M). Ultimately, H, V, and C_M were deemed to be best represented by H_{RGB} calculated from the RGB color space ($\rho = 0.56$), L from the CIE-Lab color space ($\rho = 0.73$), and $\hat{z} = Z/(X + Y + Z)$ from the XYZ color space ($\rho = -0.80$), respectively ($p < 0.001$). The corresponding explanatory powers of final NCS variables (i.e., H_{RGB}, L, and $\hat{z}$) for H, V, and C_M were 26%, 54%, and 62%, respectively ($p < 0.01$). Significant differences in $\hat{z}$ between soils identified as hydric and nonhydric, but lack of nonoverlapping ranges, indicate a potential for the NCS to complement the MSCC in assessing wetland soil color in an accessible and reproducible manner, including hydric soil identifications for wetland delineation practices. Further study with more data over various types of soils is necessary to establish stronger relationships between the NCS and MSCC. Nonetheless, the method of characterizing soil color variables from the two field methods presented in the study can serve as a template for future studies or environmental education programs desiring to use the NCS as a complement to the MSCC.

1. Introduction

Color's prominence in human observation of the environment has rendered soil color an accessible and readily apparent indicator of the structural and functional properties of soils. Soil colors are reflective

Abbreviations: ARP, Algonkian Regional Park; BR, Banshee Reeks; C, calculated; CIE, International Commission on Illumination; JJM, Julie J Metz Wetland Bank; M, measured; MN, Mason Neck; MSCC, Munsell Soil Color Chart; NCS, Nix Soil Sensor; NRCS, Natural Resources Conservation Service; USDA, United States Department of Agriculture.

* Corresponding author.
E-mail address: cahn@gmu.edu (C. Ahn).

https://doi.org/10.1016/j.scitotenv.2021.147005
0048-9697/

of, and thus serve as indicators for, organic matter content, productivity, mineralogy, and hydrologic conditions, among others (Evans and Franzmeier, 1988; Guertal and Hall, 1990; Ibáñez-Asensio et al., 2013; Ketterings and Bigham, 2000; Malone et al., 2018; Moonrungsee et al., 2015; Moritsuka et al., 2014; Pretorius et al., 2017; Sánchez-Marañón, 2011; Schwertmann, 1993; Vepraskas, 2015). Because of its link to such ecosystem attributes, soil color has been incorporated into assessments of ecosystem development: for example, the United States Department of Agriculture–Natural Resources Conservation Service (USDA–NRCS) standard for wetland delineation relies on identifying soil color to determine if soils are capable of supporting wetland ecosystems (Simonson, 1989, 1993; Vepraskas and Craft, 2016).

The Munsell Soil Color Chart (MSCC) has become a key tool in using soil color as an indicator of past and present environmental conditions by providing a means of quantifying a categorically described attribute. While the physical basis of color is derived from quantitative attributes of light, humans struggle to evaluate and communicate perceived differences of multiple colors because its perception is categorical. By providing an ordered and quantitative system to color judgments, the MSCC has thus served an essential purpose in soil science since the 1930s (Al-rasheed, 2015; Kellogg, 1937). In particular, the chart standardizes color descriptions and allows for color comparisons by noting three qualities of color: Hue (H), or spectral attribute of color consisting of red, yellow, green, blue, and purple; Value (V), or color lightness; and Chroma (C_M), or color purity (Munsell, 1905). 440 color chips of discrete hue, value, and chroma combinations, designed to resonate with perceivable color differences, span over 13 hue pages in a common version of the chart (Munsell Color, 2009; Torrent and Barrón, 1993). The adoption of the MSCC revolutionized the field of soil science by providing a standardized method of color measurement while also opening investigations into soil color relationships with environmental factors (Genthner et al., 1998; Gupta et al., 2008).

Soil color's relationship to hydrology has been thoroughly investigated to the point where a subset of soils, called *hydric soils*, have been defined based on indicators related to soil morphology, many of which rely on color. Hydric soils are defined by unique colors and patterns related to iron/manganese reduction and oxidation because they have "formed under conditions of saturation, flooding, or ponding long enough during the growing season to develop anaerobic conditions in the upper part" (Federal Register, 1994; Vasilas et al., 2018). Reddish ferric iron (Fe^{3+}) oxides typical in terrestrial soils become reduced to Fe^{2+} dissolved, and subsequently translocated within or (with enough time) below the soil profile when anaerobic conditions arise, leaving behind light and gray-colored soil grains (Richardson and Hole, 1979; Schwertmann, 1993; Schwertmann and Lentze, 1966; Simonson, 1993; Simonson and Boersma, 1972). The USDA's *Field Indicators of Hydric Soils in the United States* includes 51 indicators that outline specific soil characteristics, primarily color patterns, reflecting historical or recent hydrological conditions that indicate the soil is in fact a hydric soil (Vasilas et al., 2018). While wetland delineation and monitoring incorporate hydrologic, vegetative, and soil aspects (Tiner, 2017), soils are particularly informative: they can respond more swiftly than vegetation to changing hydrology, but also form lasting morphological features that indicate long-term conditions even after saturation, flooding, or ponding conditions disappear (He et al., 2003; Vepraskas et al., 2004; Vepraskas and Lindbo, 2012).

Many hydric soil field indicators designate thresholds of H, V, and C_M to discriminate between hydric and nonhydric soils. For example, over 10 indicators identify a soil as hydric based on the presence of iron and/or manganese depletions, defined as "bodies of low chroma (2 or less) having a value of 4 or more where Fe-Mn oxides have been stripped …"; identifying depletions thus requires both $C_M \leq 2$ and $V \geq 4$. Furthermore, almost all indicators require certain soil layers to "have a dominant chroma of 2 or less" (Vasilas et al., 2018). Field and laboratory studies have corroborated that anaerobic environments capable of supporting wetland ecosystems will produce low-chromas soils ($C_M \leq 2$) when initial iron concentrations are sufficient (Vepraskas, 2015). In conjunction with hydric soil field indicators, the MSCC thus serves as a bridge between human observations of color and the capacity to identify wetland soils.

The MSCC is not without its disadvantages; for decades, one of the foci within soil science has been researching alternative methods of soil color determination that can complement or supersede the MSCC. Color readings using the MSCC are based on human judgment, and the MSCC requires training and practice to increase accuracy and diminish user-based variability in color determinations. Thus, while laypeople unfamiliar with the MSCC may be able to perceive soil colors, they cannot easily utilize the MSCC for accurate rapid soil color determination. Additionally, MSCC color readings are affected by manufacturing variability, lighting conditions affected by time of day and weather, MSCC aging over time, and anatomical and psychological differences between individuals perceiving colors (Fairchild, 2013; Rabenhorst et al., 2015; Sánchez-Marañón et al., 2011).

Given these shortcomings, a subset of soil studies concerned with soil color have focused on field alternatives to the MSCC, including handheld colorimetry (Campos and Demattê, 2004), spectroscopy (Shields et al., 1966; Summers et al., 2011; Torrent and Barrón, 1993; Viscarra Rossel et al., 2009; Jones and McBratney, 2016), and digital photography using medium- to high-end cameras and mobile phone cameras (Aitkenhead et al., 2016; Fan et al., 2017; Gómez-Robledo et al., 2013; Han et al., 2016; Moonrungsee et al., 2015; O'Donnell et al., 2010; Viscarra Rossel et al., 2008). While most alternatives are not field-based, app-based color measurement instruments like the Nix Color Sensor (NCS) may provide a means of field-based color determination that is resistant to the human judgment and subjective aspects of MSCC readings. The NCS uses a highly consistent pre-calibrated LED light to scan a surface, which is isolated from ambient light by the sensor's diamond shape and 1.5 cm diameter aperture (Schmidt and Ahn, 2019). When a surface is scanned, colors are automatically measured, transmitted to a Bluetooth-linked smartphone app, and stored. In contrast to the MSCC, the NCS offer a promising avenue of rapidly identifying soil colors without requiring experience and familiarization or additional data recording. It has been successfully deployed in nonhydric soil color determination and education endeavors; promising findings of its accuracy encourage further investigation into its utility for hydric soil identification (Stiglitz et al., 2016a, 2016b; Stiglitz, Mikhailova, Post, Schlautman, & Sharp, 2017; Stiglitz, Mikhailova, Post, Schlautman, Sharp et al., 2017).

The goal of this study was to better understand how the NCS can complement and/or act as a substitute for the MSCC in observing soil color. We investigated if the NCS can identify hydric soils, as identified by hydric field indicators reliant on the MSCC, for the purpose of wetland delineation. We observed and analyzed soil colors in forested ecosystems with mapped hydric soils in Northern Virginia using both the MSCC and NCS. The main objectives were: (1) to create a methodology to characterize color variables used by the NCS and compare them with those of the MSCC; (2) to assess correlations between MSCC and NCS variables for soil colors in order to identify the most suitable NCS variable(s) to represent each of the three commonly observed Munsell variables (H, V, and C_M); (3) to investigate the explanatory power of each NCS variable for respective MSCC variables through regression; and (4) to better understand if the NCS can aid in discriminating between hydric and nonhydric soil colors as identified through use of the MSCC.

2. Materials and methods

2.1. Site description

The study was conducted at four wetland sites within Northern Virginia, all located in the Chesapeake Bay Watershed: Mason Neck Wildlife Refuge (MN) in Fairfax County, Julie J. Metz – Neabsco Creek Wetland Bank (JJM) in Prince William County, and Banshee Reeks

Nature Preserve (BR) and Algonkian Regional Park (ARP) in Loudoun County (Fig. 1). Similar to the previous years, average temperatures were 56.3 °F (7 °F to 95 °F) in 2018 and 57.2 °F (−2 °F to 100 °F) in 2019; total precipitation was 169.5 cm in 2018 and 103.7 cm in 2019, with 2018 being the wettest year of the decade by over 50 cm (Menne et al., 2012).

Both MN and JJM sites fall within the Coastal Plain physiographic region of Northern Virginia. The four study plots at MN (38° 38′ 28″ N, 77° 9′ 54″ W) belong to a hardwood forest and palustrine forested wetland with rolling microtopography consisting of high points (hummocks) and low points (hollows) adjacent to a riverine freshwater marsh. Hydrologic inputs originate primarily from precipitation. Hollow locations are composed of the hydric Gunston silt loam and experience occasional to frequent standing or flowing water, depending on seasonal weather patterns (Ahn et al., 2009). Hummock locations, mapped as the nonhydric Matapeake silt loam and Mattapex loam, are conversely rarely to never ponded or flooded (USDA–NRCS Soil Survey Staff, 2020a). Adjacent to Neabsco Creek near the Potomac River, JJM (38° 36′ 25″ N, 77° 16′ 34″ W) is the first created mitigation wetland in the nation and contains both tidal and nontidal sections. Monitoring up to 20 years after its creation in 1994 confirmed the presence of wetland hydrologic conditions per the Army Corps of Engineers wetland delineation manual (Environmental Laboratory, 1987; Wetland Studies and Solutions Inc., 2020). Several plots are flooded year-round, whereas others experience frequent to occasional surface saturation. Soils at JJM plots are mapped as hydric and include the very poorly drained Featherstone mucky silty loam and the Hatboro-Codorus complex (USDA–NRCS Soil Survey Staff, 2020c). Plots receive water inputs from a range of hydrologic sources such as tidal freshwater, groundwater recharge, precipitation, and stream surface flow.

BR (39° 1′ 48″ N, 77° 35′ 46″ W) and ARP (39° 3′ 25″ N, 77° 21′ 50″ W) fall within the Piedmont physiographic region. BR plots experience occasional to frequent flooding or ponding, and have been mapped to contain both the hydric Albano silt loam as well as the nonhydric Codorus and Manassas silt loams (Fuller, 2007; USDA–NRCS Soil Survey Staff, 2020b). Plots have dynamic hydrologic characteristics: some regions of the preserve are primarily influenced by groundwater connection with subsurface flow from Goose Creek, while others primarily receive inputs from precipitation and surface runoff near small tributaries of Goose Creek (Paul, 2017). Finally, ARP plots along the Sanctuary Trail occur within riparian forests, freshwater forested wetlands, and at the fringes of a freshwater emergent wetland. Mapped soil series include the Rowland silt loam on floodplains and Lindside silt loam on terraces; while neither is classified as hydric, vegetative and hydrologic scouting before sampling began indicated a propensity of flooding and/or ponding at plots to support wetland vegetation (USDA–NRCS

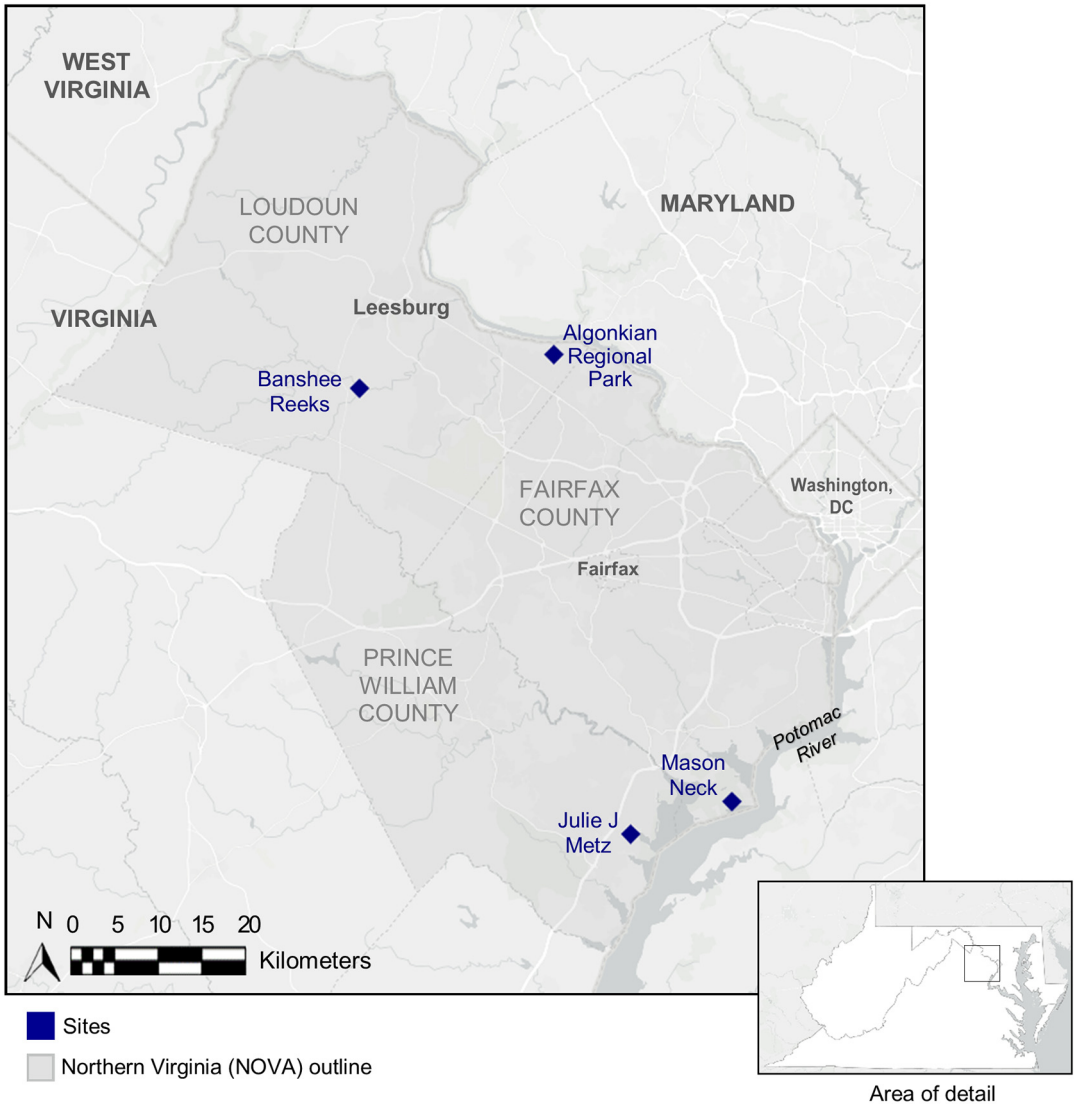

Fig. 1. Regional map displaying the four study sites located in Northern Virginia (NOVA), USA.

Soil Survey Staff, 2020b). Water inputs include overland flow from the Potomac River, overland flow and groundwater connection with nearby emergent wetlands, and precipitation. Water tables range from 0 cm near emergent habitat and reach 60 cm within forested floodplains (US Fish and Wildlife Service, 2010).

2.2. Soil collection

Per site, 4 to 5 randomly selected plots (each 1 m × 1 m) were visited in March–April, June–July, and August–September of 2018 and 2019 for soil sampling. A 10-cm diameter auger (AMS) was used for soil profiling; while augering cannot provide an in-tact and undisturbed core from sampling, it provides an adequate sample size for identifying present redoximorphic features in a relatively short time period without large plot disturbance, allowing it to be scaled to both professional and nonprofessional soil investigations (O'Donnell et al., 2011).

After removing surface debris, soil was collected from each plot. Given variability in plots' soil textures, moisture, and compactness, a variable amount of soil ranging from 10 to 30 cm in depth was removed at a time and laid on a white sheet to reflect in-situ soil horizonation. Concurrent measurement of soil depth was conducted, and every 5 to 10 cm interval was noted to establish depth markers. While peds were naturally separated during transfer from the auger to the sheet, care was taken to maintain in-situ ordering. After all 60 cm of soil had been sampled and transferred, color recordings began.

Only interior colors were examined as to avoid including smudged colors in the readings. Starting at the top of the profile, each ped was broken in half. For each ped, the two halves were inspected for interior colors, and colors were recorded using both the MSCC and the NCS at each site visit. When scanning matrix colors, relatively flat surface areas of the peds were chosen for NCS scanning to reduce sources of error. After colors were recorded, each half was iteratively broken along structural voids to form smaller peds. At each stage of the process, newly exposed interior soils were visually scanned for new colors; when new colors were identified, MSCC and NCS colors were recorded. This process was repeated to a ped diameter of roughly 3–5 cm. Color readings did not go past the 3–5 cm diameter ped size for either the MSCC or NCS because of the size of the aperture of the NCS (~1.5 cm): as the NCS requires a planar surface to ensure the edges surrounding its aperture are tightly touching the surface of color recording, smaller fractions (e.g., diameter < 3–5 cm) risk the introduction of uneven interior and edge surfaces which would introduce error into the measurements. Per initial ped, this required about 3 to 5 steps of halving.

This process was repeated for all peds down to 60 cm; however, for peds of the same horizon with visible equivalences in interior matrix and RMF colors, MSCC and NCS color recording were not repeated. When possible, surfaces were smoothed using pressure to create an even surface for measuring color with the NCS; this was not always possible when physical pressure affected the visibility of the color. The identification and recording of each color took one to two minutes for the MSCC, and one minute or less for the NCS.

2.3. Determination of soil colors

For each identified color, 18 measured (M) variables were collected: 3 from the MSCC (H, V, and C_M), and 15 from the NCS (L, a, b, C, h, X, Y, Z, R, G, B, C_K, M_K, Y_K, and K_K). Per color, the three variables from the Munsell color space (H, V, and C_M) and the 15 variables from the NCS were measured and recorded (Table 1). Procedures for MSCC use were followed, such as reading soil colors from the chart in daylight and with moist soil samples. While specific "gley" or bluish gray or greenish gray colors with low chroma ($C_M \leq 2$) and high value ($V \geq 4$) are common to wetland soils and were observed, they were not included in the analysis given their coincidence with high soil moisture that, in the context of the data set, reduced replicability and reproducibility.

As hue is an alphanumeric variable (e.g., "10YR"; Fig. 2) a numeric variable H# was recorded as a quasi-equivalent expression to aid in statistical analyses. H# was recorded by denoting hues with negative values equal to numerical distances from 10R if redder than 10R (5R and 7.5R), and with positive values equal to numerical distances from 10R if yellower than red (2.5YR to 5Y). Thus, H# = −5 for 5R and 15 for 5Y (Kirillova et al., 2015). All further discussion of MSCC variables used in statistical analyses relies on the "measured" (M), or directly measured, variables H# (as a proxy for H), V, and C_M.

The NCS was concurrently used to measure all identified colors with the exception of those unable to fit within the NCS aperture (e.g., color feature diameters < 1.5 cm). Measurements were made in triplicate by moving the sensor to three areas of a perceptually uniformly colored soil fraction. To record and store colors, the NCS was connected to a smartphone running the Nix Pro Color Sensor app, which automatically recorded and stored scanned colors alongside timestamps and typed descriptors. The use of the NCS and resulting color measurement were stored on the smartphone app and exported in a CSV file (Fig. 2). Each color measurement made by the NCS is automatically represented as 15 measured variables from five color spaces: (1) The International Commission on Illumination (CIE) Lab, or CIE-Lab; (2) CIE-LCh, which shares the variable L with the CIE-Lab space; (3) CIE-XYZ; (4) the RGB model (including color spaces RGB, sRGB, and Lin.sRGB) commonly used with digital displays; and (5) CMYK (Table 1). Each space is named according to the variables which define colors in said space; for example, a color defined in the LCh space is represented as a three-dimensional vector composed of an L dimension, a C dimension, and an h dimension, respectively. For the purposes of this study, only the first RGB space data was utilized from the RGB color model. More information on the genesis and applicability of these color spaces is outlined in Viscarra Rossel et al. (2006).

2.4. Formulation of calculated variables

Calculated (C) variables were identified as a relatively rapid and accessible method for arithmetically manipulating measured MSCC and NCS variables to increase the potential likelihood for moderate to strong relationships to surface between the two methods. A list of calculated variables to consider was produced from color science literature indicating the formulation of color-relevant variables from measured color space variables. For NCS color variables, calculations were based in literature recommendations on (1) the de-correlation of linearly dependent color variables and the reduction of color space dimensions; and (2) the basis of absent color spaces non-identical but linked to the color spaces provided by the NCS. In all cases, measured variables from one color space were used as the basis of derivation for each new variable.

2.5. Processing of soil color data

For the set of measured (n = 18) and final calculated variables (n provided in Section 3.2), descriptive and normality statistics were conducted on all variables using Microsoft® Excel 2013 to better understand variable distribution. Next, a stepwise investigation of variable relationships was conducted via Spearman correlation analysis to yield a final list of one NCS variable most capable of relating to MSCC variables representative of H, V, and C_M. The analysis contained two key procedures: the identification of strong Spearman correlation coefficients (ρ) for MSCC-NCS variable pairs, and the removal of variables with high intra-method (MSCC-MSCC or NCS-NCS) correlations, i.e., collinearity, from further consideration.

Correlation coefficients were studied between all measured and calculated MSCC variables and (1) all measured NCS variables plus (2) final calculated NCS variables. Generally, 0.70 is accepted as a threshold separating moderately strong from strong relationships (Akoglu, 2018; Dancey and Reidy, 2007; Mukaka, 2012); thus, strong correlations, i.e., those with $|\rho| \geq 0.70$, were flagged for further analysis. If the

Table 1
Summary of all measured and calculated color (space) variables obtained using the Munsell Soil Color Chart (MSCC) and Nix Color Sensor (NCS).

Measured or calculated [b]	Instrument	Color space	Description	Variable name	Label	Variable description (where applicable)	Range for common soil colors
Measured	Munsell Soil Color Chart (MSCC)	Munsell	Perceptually linear color space with 24 categorical color hues and discrete and independent luminance and chromatic variables	Hue (Alphanumeric) [a]	H	Spectral attribute of color (yellow, red, green, blue, purple); the MSCC is composed of 9 main pages relating to distinct hues in steps of 2.5: - red: 5R, 7.5R, 10R - yellow-red: 2.5YR, 5YR, 7.5YR, 10YR yellow: 2.5Y, 5Y	5R through 10Y 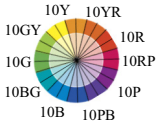
				Hue (Numeric)	H#	Linear ranking of MSCC hues, where 10R=0. Each 2.5-unit increase in H equates to a 2.5-step decrease (redder) or increase (yellower) from 0 10R = 0; 2.5YR = 2.5; 5YR = 5 7.5YR = 7.5; 10YR = 10; 2.5Y = 12.5; 5Y = 15	2.5 to 15 (5Y)
				Value	V	Lightness of color (0=black, 10=white)	0 – 8
				Chroma	C_M	Intensity or purity of color (0=achromatic)	0 – 8
	Nix Color Sensor (NCS)	CIE Lab [d]	Device-independent color space that separates luminance and chromatic components of color	L*	L	Lightness	0 - 100
				a*	a	Chromaticity, where -: green; +: red	Hue dependent
				b*	b	Chromaticity, where - : blue; + : yellow	Hue dependent
		CIE XYZ	Device-independent color space which includes virtual components X and Z	X	X	Virtual and nonnegative mix of shorter- and higher-wavelength light; orthogonal to Y	Hue dependent; 0 – 15
				Y	Y	Luminance	Hue dependent
				Z	Z	Shorter-wavelength light (corresponds to blue)	Hue dependent
		CIE LCh [c, d]	Device-independent color space which separates luminance and chromatic variables	L*	L	Lightness	0 - 100
				C*	C	Chroma	0 - 100
				h*	h	Hue	0 – 360 (degrees)
Measured	Nix Color Sensor (NCS)	RGB, sRGB, Lin.sRGB	Additive and device-dependent cube-shaped space	R	R	Red	0 - 255
				G	G	Green	0 – 255
				B	B	Blue	0 – 255
		CMYK	Subtractive space used for printing	C	C_K	Cyan	0 - 100%
				M	M_K	Magenta	0 - 100%
				Y	Y_K	Yellow	0 - 100%
				K	K_K	Black	0 - 100%
Calculated		CIE XYZ	Device-independent color space which includes virtual components X and Z	X / (X+Y+Z)	$\hat{x}$	Proportion of X in X+Y+Z	0 – 1
				Y / (X+Y+Z)	$\hat{y}$	Proportion of Y in X+Y+Z	0 – 1
				Z / (X+Y+Z)	$\hat{z}$	Proportion of Z in X+Y+Z	0 – 1
		RGB, sRGB, Lin.sRGB	Additive and device-dependent cube-shaped space	(2G – R – B)/4	H_{RGB}	Linear combination of G, R, and B to produce linear independence (Viscarra Rossel et al., 2006)	-25 – 25
				(R + G + B)/3	I_{RGB}	Linear combination of G, R, and B to produce linear independence (Viscarra Rossel et al., 2006)	30 – 200
				(R – B)/2	S_{RGB}	Linear combination of R and B to produce linear independence (Viscarra Rossel et al., 2006)	0 – 80
		CMYK	Subtractive space used for printing	$C_K - Y_K$	Co	Linear combination of C_K and Y_K to produce linear independence (Malvar et al., 2008)	-1 – 0
				$Y_K + (C_K - Y_K)/2$	Cg	Linear combination of C_K and Y_K to produce linear independence (Malvar et al., 2008)	0.50 – 0.75
				$1 – (2M_K + Y_K + C_K)/4$	Ym	Linear combination of M_K, C_K and Y_K to produce linear independence (Malvar et al., 2008)	0.25 – 0.75

(a) H is an inherent variable of the MSCC but is not included in statistical analyses or variable counts mentioned in results and discussion.
(b) Measured variables were directly measured using the prescribed method (MSCC or NCS); calculated variables required arithmetical operations (addition, subtraction, multiplication, and/or division) to combine multiple variables belonging to a single color space into one variable.
(c) While total number of measured variables from the NCS sums to 16 from this table, L is a part of CIE-Lab and CIE-LCh color spaces; thus there are 15 measured NCS variables. d The asterisks that follow the alphabetical notations of the CIE variables L*, a*, b*, C*, and h* are inherent aspects of the variable names and are not additions relevant to a footnote.

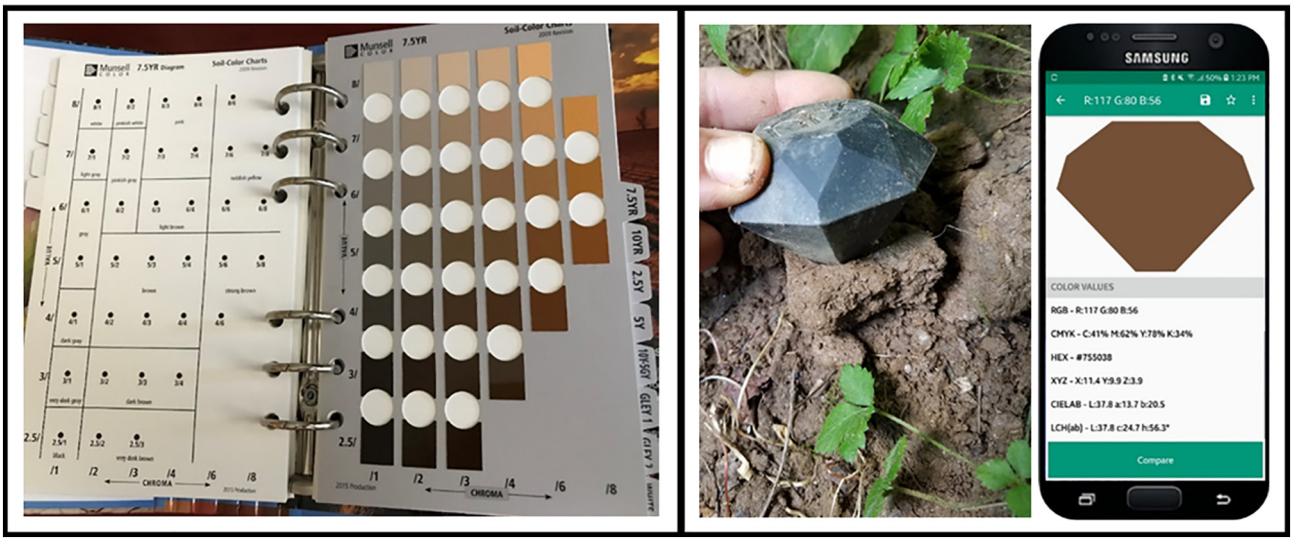

Fig. 2. Demonstration of color measurements in the field using the Munsell Soil Color Chart (MSCC; left) and the Nix Color Sensor (NCS) paired with the smartphone app (right).

threshold was not met by at least one NCS variable for either H, V, or C_M variables, the threshold was lowered in steps of 0.05 until at least one NCS variable met the threshold. Strong ($|\rho| \geq 0.70$) correlations with V and C_M variables, and modest ($|\rho| \geq 0.50$) correlations with H variables, were subsequently flagged. NCS and MSCC variables showing zero strong or modest correlations with variables of the opposing method (i.e., MSCC and NCS, respectively) were removed.

Intra-method variable redundancy was identified by flagging very strong MSCC-MSCC and NCS-NCS correlations ($|\rho| \geq 0.90$), i.e., collinear pairs (Mukaka, 2012; Schober et al., 2018). Where one collinear variable was more strongly correlated with variables of the opposing method ($|\Delta\rho| > 0.02$), all other collinear variables were removed. Where collinearity was found between variables that shared similar correlation coefficients with variables of the opposing method ($|\Delta\rho| \leq 0.02$), the following ordered criteria were used to give preference to: (1) measured over calculated variables; (2) variables commonly used in the literature (e.g., L for V) (Mahyar et al., 2010; Marqués-Mateu et al., 2015; Moonrungsee et al., 2015; Torrent and Barrón, 1993; Viscarra Rossel et al., 2006; Yang et al., 2001); and (3) visual goodness of fit of scatterplots when plotted against the most highly correlated variable of the opposing method. A similar set of criteria were subsequently used to eliminate all but one NCS variable per H, V, and C_M variables—i.e., yielding three variable pairs. Maximal $|\rho|$ was used as the single criterion to choose between variable pairs for a given MSCC variable when $|\Delta\rho| > 0.02$. Where $|\Delta\rho| \leq 0.02$, one MSCC-NCS variable pair was chosen with preference using the three criteria.

For final MSCC-NCS variable pairs, simple linear regressions were conducted to identify explanatory or predictive power of each NCS variable with respect to its MSCC pair using r^2 statistics (at $p < 0.01$). Regression models with $r^2 \geq 0.50$ were assessed to be adequate, as this threshold is common for appropriately identifying predictor variables that outweigh other noncontrolled variables or sources of error (e.g., Sanyal et al., 2017). For regression models that were deemed inadequate (i.e., $r^2 < 0.50$), the dataset was split by physiographic region (Coastal Plain - MN and JJM; Piedmont - BR and ARP) to identify if more control over soil texture—where Coastal Plain sites are sandier—would improve predictive power.

Additionally, colors were separated into two sets: one with colors that, after MSCC readings, satisfied a necessary condition of any hydric soil field indicator (e.g., depleted matrix colors; prominent concentration colors; gley colors; $n = 162$) and those not indicative of hydric soils (e.g., faint concentration colors; non-depleted or reduced matrices; $n = 57$) (Vasilas et al., 2018). Using these datasets, descriptive statistics and 2-sample *t*-tests were conducted on V and C_M, plus final Nix variables related to V and C_M (total $n = 4$), to compare colors related to hydric soils ("hydric") versus colors not related to hydric soils ("nonhydric").

3. Results

3.1. Describing measured variables for MSCC and NCS

3.1.1. Measured MSCC variables

The MSCC contains 9 hue pages most commonly used by MSCC users representing quarter-steps of Munsell hues red (R), yellow-red (YR), and yellow (Y), and are ordered from 5R (most red) to 5Y (most yellow) (Table 1). Each page includes up to 40 color chips with discrete values for V (vertical axis) and C_M (horizontal axis) each ranging from 0 up to 8 depending on hue (Table 1). Higher V corresponds to lighter colors; higher C_M corresponds to purer colors (Fig. 2; Table 1). C_M and V are discrete variables denoted as whole numbers (0, 1, 2, 3, …, 8). Half-step judgments are possible, but not easily judged, between each unit.

3.1.2. Measured NCS variables

The color spaces included in the NCS app represent common color spaces and variables used across color science and color-related subdisciplines. While some NCS variables are meaningless in terms of perceptual attributes of color such as hue or saturation (e.g., the virtual X from the XYZ color space), most variables are related to properties of hue, value, and/or chroma (Table 1). L (CIE-Lab and CIE-LCh) corresponds to lightness like MSCC V, with lower numbers representing darker colors. The Lab variables a and b provide a green (−a) to red (+a) and yellow (−b) to blue (+b) spectrums of hues. The LCh space is similar to the Munsell space, with variable meanings for L (V), C (C_M), and h (H) directly linking to those of their MSCC counterparts. CMYK and RGB color spaces have variables related to specific hues—cyan, magenta, yellow, and black for CMYK, and red, green, and blue for RGB. For each of these color spaces, all variables encompass a quality of lightness and are not linearly independent. For example, in the RGB (red, green, and blue) color space, a unit-increase for each variable relates to an overall lightening of color, as the red, green, and blue components "add" to increase lightness. The opposite is true of the subtractive CMYK (cyan, magenta, yellow, and black) color space.

3.2. Calculation of variables to increase MSCC-NCS variable pairs

The method of identifying calculated variables relevant for relating NCS and MSCC measurements led to an expansion of measured

(M) variables (MSCC: n = 3; NCS: n = 15) to include an additional 9 calculated (C) variables (MSCC: n = 0; NCS: n = 9), yielding 27 total variables (Table 1).

For the MSCC, three calculated variables were considered for analysis—angular hue, or H°, which represents hues as angles on a circular color wheel; sinH°; and cosH° (Schmidt and Ahn, 2019). However, none were deemed useful for this study's application. Because angular hue (H°) was defined with 5R set equal to 0° (Ruck and Brown, 2015; Sánchez-Marañón et al., 2011), it shared a direct linear relationship with H# and added no value to the study. Additionally, while sinH° and cosH° could have benefited our research aims, they were redundant: the dataset only included hue calculations for H# that, when transformed to H°, fell within quadrant one (i.e., yielding monotonic changes to both cosH° and sinH°, respectively). Indexing H# and H° differently and independently (e.g., 5R = 0 for H# but 10R = 0° for H°) was deemed unnecessary and nonproductive due to the absence of colors with hues redder than 2.5YR (e.g., 10R, 7.5R, …; n = 0). For soils of Northern Virginia which are not often redder than 5YR, it was determined that derivations of MSCC variables are simply not necessary to augment the color information provided by MSCC.

With respect to V and C_M, zero calculated variables were deemed suitable for relating NCS-measured colors to MSCC-measured colors. While other calculations exist in the literature, transformations that characterize soil color patterns instead of color (e.g., redoximorphic features) or combine variables into multivariable expressions do not serve the need of linking NCS color variables to the MSCC color aspects hue, value, and chroma. Thus, arithmetic operations including more than one of H, V and C_M or relating to color patterns instead of colors were deemed unsuitable (Evans and Franzmeier, 1988; Jien et al., 2004; Thompson and Bell, 1996).

In contrast to the MSCC, calculated variables (C) derived from the NCS measured variables were deemed useful to color relationship studies between the NCS and the MSCC. RGB and CMYK include dependent variables; thus, linearly independent variables from the RGB and CMYK color space were calculated from transformations delineated by Malvar et al. (2008). The derived variables provide a simple algebraic transformation of R, G, and B and C_K, M_K, Y_K, and K_K, respectively, and have been shown to be useful in color science (Malvar et al., 2008; Viscarra Rossel et al., 2006). Calculations to normalize the XYZ color space and create variables used in the CIE-xyY color space, not included in NCS measurements, were also made (Viscarra Rossel et al., 2006).

This approach led to the inclusion of 9 calculated variables for the NCS: (1–3) $\hat{x}$, or X / (X + Y + Z); $\hat{y}$, or Y / (X + Y + Z); and $\hat{z}$, or Z / (X + Y + Z) from the XYZ color space; (4–6) H_{RGB}, or $(2G - R - B) \cdot 4^{-1}$; I_{RGB}, or $(R + G + B) \cdot 3^{-1}$; and S_{RGB}, or $(R - B) \cdot 2^{-1}$ from the RGB color space; and (7–9) Co, or $C_K - Y_K$; Cg, or $Y_K + [(C_K - Y_K) \cdot 2^{-1}]$; and Ym, or $1 - [(2M_K + Y_K + C_K) \cdot 4^{-1}]$ from the CMYK color space. The XYZ color space variables provide chromaticity coordinates between 0 and 1 and provide a means of including the CIE Yxy color space in the analysis. While Z / (X + Y + Z) is usually ignored in color sciences due to its linear dependence with X / (X + Y + Z) and Y / (X + Y + Z), it is included here as not all normalized variables were to be used in concert.

3.3. Describing observed colors through MSCC and NCS variables

Descriptive statistics for all measured (n = 3) MSCC variables indicate H# ranged from 2.5 (=2.5R) to 15 (=5Y) with a mean of 8.4, or 8.4YR; this most closely mirrors the MSCC hue page 7.5YR, with H# (7.5YR) = 7.5 (Table 2). V ranged from 2 to 7 with a mean of 4.3 ± 0.1, and C_M ranged from 1 to 6 with a mean of 3.1 ± 0.1. Measured variables V and C_M were nonnormal per the Shapiro test for normality ($p < 0.001$).

Descriptive and normality statistics for all measured (n = 15) and calculated (n = 9) NCS variables indicate that L and R were the only measured variables to display normal distributions per the Shapiro test (p > 0.05; Table 2). Additionally, X and Y from the XYZ color space were almost identically distributed with similar means, medians, ranges, and skewness and kurtosis. From R, G, and B, B displayed the lowest range and did not surpass 99 out of a possible 355. At the α =

Table 2
Descriptive statistics for all measured and calculated variables from the Munsell Soil Color Chart (MSCC) and Nix Color Sensor (NCS) used in this study.

Variable type	Color space	Variable	Shapiro normality[a]	Median	Mean ± SE	Kurtosis	Skewness	Range	(Min, Max)
Measured	MSCC	H#	<0.001	7.5	8.4 ± 0.2	−0.328	−0.083	12.5	(2.5, 15)
		V	<0.001	4	4.3 ± 0.1	−0.363	−0.074	5.0	(2, 7)
		C_M	<0.001	3	3.1 ± 0.1	−0.327	0.154	5.0	(1, 6)
	NCS – Lab	L	0.113†	36.7	37.6 ± 0.7	−0.271	−0.016	47.4	(13.2, 60.5)
		a	0.010*	7.9	7.9 ± 0.2	−0.787	0.205	12.7	(1.9, 14.6)
		b	0.006	16.0	16.8 ± 0.4	−0.830	0.223	22.4	(5.4, 27.8)
	NCS – LCh	C	0.002	18.4	18.7 ± 0.4	−1.062	0.022	23.5	(6.2, 29.7)
		h	<0.001	65.3	64.9 ± 0.5	−1.206	0.202	24.3	(54.6, 78.9)
	NCS – XYZ	X	<0.001	10.3	11.5 ± 0.4	0.335	0.782	28.0	(1.7, 29.6)
		Y	<0.001	9.4	10.8 ± 0.4	0.469	0.875	27.1	(1.6, 28.7)
		Z	<0.001	4.2	4.9 ± 0.2	0.029	0.787	11.0	(0.9, 12.0)
	NCS – RGB	R	0.629†	108	107.8 ± 1.9	−0.330	−0.039	131	(40, 171)
		G	0.006	81	83.9 ± 1.6	−0.296	0.243	108	(32, 140)
		B	0.009	60	61.9 ± 1.2	−0.431	0.168	73	(26, 99)
	NCS – CMYK	C_K	<0.001	0.47	0.47 ± 0.06	−0.552	0.132	0.32	(0.32, 0.64)
		M_K	<0.001	0.60	0.58 ± 0.06	−0.170	−0.829	0.27	(0.41, 0.67)
		Y_K	0.002	0.74	0.73 ± 0.04	0.724	−0.536	0.23	(0.60, 0.83)
		K_K	0.005	0.36	0.35 ± 0.14	−0.280	0.339	0.70	(0.06, 0.76)
Calculated	NCS – XYZ	$\hat{x}$	0.045*	0.405	0.423 ± 0.001	−0.075	−0.229	0.086	(0.377, 0.462)
		$\hat{y}$	0.008	0.467	0.396 ± 0.001	−0.449	0.320	0.036	(0.381, 0.416)
		$\hat{z}$	0.001	0.178	0.181 ± 0.002	−0.217	0.465	0.105	(0.135, 0.240)
	NCS – RGB	H_{RGB}	<0.001	−0.25	−0.50 ± 0.12	−0.798	0.154	6.75	(−3.50, 3.25)
		I_{RGB}	0.082*	82.7	84.5 ± 1.45	−0.322	0.064	103	(32.7, 136.0)
		S_{RGB}	<0.001	22.5	22.9 ± 0.5	−1.034	0.062	31.5	(7.0, 38.5)
	NCS – CMYK	Co	0.003	−0.266	−0.267 ± 0.006	−0.777	0.234	0.340	(−0.410, −0.070)
		Cg	<0.001	0.599	0.599 ± 0.003	0.268	−0.124	0.170	(0.505, 0.675)
		Ym	<0.001	0.403	0.413 ± 0.003	0.035	−0.697	0.210	(0.333, 0.543)

[a] Shapiro normality refers to the p-value obtained from the Shapiro test for normality; variables assuming statistically significant p values where $p < 0.01$ (without individual footnotes) are non-normally distributed.
† Shapiro p-value is not significant (p > 0.10), indicating the variable is normally distributed.
* Shapiro p-value is significant at 0.01 < p < 0.10, indicating the variable is likely to be non-normally distributed.

Table 3
Spearman correlation matrix for all measured color variables from the Munsell Soil Color Chart (MSCC) and Nix Color Sensor (NCS) used in this study.

Nix Color Sensor – measured (n = 15)	Munsell Soil Color Chart – measured (n = 3)		
	H#	V	C_M
L	0.31	**0.73**[a]	0.39
a	−0.24	0.15	0.60
b	0.20	0.61	**0.76**[a]
C	0.12	0.56	**0.77**[a]
h	*0.54*[b]	0.44	−0.08
X	0.29	**0.73**[a]	0.43
Y	0.31	**0.73**[a]	0.39
Z	0.32	0.66	0.18
R	0.25	**0.72**[a]	0.49
G	0.33	**0.73**[a]	0.34
B	0.32	0.63	0.12
C_K	−0.13	−0.62	−0.67
M_K	−0.47	−0.63	−0.13
Y_K	−0.11	−0.06	0.53
K_K	−0.31	**−0.73**[a]	−0.37

Note. All correlations with $|\rho| \geq 0.21$ are significant at $p < 0.001$.
[a] Boldface indicates $|\rho| \geq 0.70$.
[b] Italics indicate $|\rho| \geq 0.50$ (only highlighted for MSCC H#).

0.10 level, all calculated variables were significantly nonnormal. H_{RGB} and Co were primarily negative whereas I_{RGB}, S_{RGB}, Cg, and Ym consisted exclusively of positive values.

3.4. Correlation

3.4.1. Pre-screening results: MSCC-NCS variable correlations

An assessment of Spearman correlations between MSCC variables (n = 3) and measured NCS variables (n = 15) highlighted that NCS variables a, Z, B, C_K, M_K, and Y_K failed to hold strong (V, C_M) or modest (H) correlations with MSCC variables (Table 3). These variables were thus removed from further analysis. H# was modestly correlated with h only ($|\rho| = 0.53$; $p < 0.001$). V was strongly positively correlated with L, X, Y, and G ($\rho = 0.73$) and strongly negatively correlated with K_K ($\rho = -0.73$); V also showed strong correlation with R ($\rho = 0.72$) ($p < 0.001$). C_M was strongly correlated with b ($\rho = 0.76$) and C ($\rho = 0.77$) ($p < 0.001$).

Several variable sets displayed high intra-method (MSCC-MSCC or NCS-NCS) correlations: (1) L, X, Y, Z, R, G, B, and K_k and (2) C and b. The collinearity criteria of Section 2.5 were used to remove NCS variables X, Y, R, G, K_K from further analysis. In conjunction with NCS variables removed for failing to hold strong (V, C_M) or modest (H) correlations with NCS variables, NCS variables L, C, and h remained for further analysis, and remaining correlation pairs were V and L; C_M and C; and H# and h.

Between all MSCC variables (n = 3) and calculated NCS variables (n = 9), $\hat{z}$, H_{RGB}, I_{RGB}, and Co displayed strong (H) or modest (V, C_M) correlations with MSCC variables; $\hat{x}$, $\hat{y}$, S_{RGB}, Cg, and Ym were only weakly (H) or moderately (V, C_M) correlated with MSCC variables and were thus removed from further analysis (Table 4). H_{RGB} was modestly correlated with H# ($\rho = 0.56$). V was not more strongly correlated with calculated NCS variables than measured NCS variables; the maximum coefficient was $\rho = 0.72$ between V and I_{RGB} ($p < 0.001$). C_M showed strong correlations with $\hat{z}$ ($\rho = -0.80$), Co ($\rho = -0.80$) and S_{RGB} ($\rho = 0.74$) ($p < 0.001$). No pairs of NCS calculated variables were highly collinear ($|\rho| < 0.90$). Given the remaining four calculated NCS variables, strong (V, C_M) and modest (H) correlation pairs were V and I_{RGB}; C_M and $\hat{z}$; C_M and S_{RGB}; C_M and Co; and H# paired with H_{RGB}.

3.4.2. Choosing final variables

From the remaining MSCC-NCS variable pairs for H, selection criteria were employed to choose between H#-h and H#-H_{RGB}. Comparing the scatterplots of similarly correlated pairs H#-H_{RGB} and H#-h ($|\Delta\rho| \leq 0.02$; Tables 3 and 4), H_{RGB} was chosen as the most suitable variable for relating to MSCC H. Next, to choose between V-L and V-I_{RGB} ($|\Delta\rho| \leq 0.02$; Tables 3 and 4), L was chosen over I_{RGB} due to being a measured versus calculated variable as well as its prevalence in soil and color science literature. Finally, for C_M correlations with b, C, $\hat{z}$, Cg, and Co, C_M-$\hat{z}$ and C_M-Co were most strongly correlated than the other pairs ($|\Delta\rho| > 0.02$). Scatter was similar between C_M vs. $\hat{z}$ and C_M vs. Co plots. Ultimately, $\hat{z}$ was selected due to the relationship between $\hat{z}$ and the pre-established CIE-xyY (or $\hat{x}\hat{y}$Y using our notation), a color space discussed in color science literature where $\hat{z} = 1 - (\hat{x} + \hat{y})$ (Viscarra Rossel et al., 2006).

Table 4
Spearman correlation matrix between all measured Munsell Soil Color Chart (MSCC) variables and all calculated variables from the Nix Color Sensor (NCS) used in this study.

Nix Color Sensor – calculated (n = 9)	Munsell Soil Color Chart – measured (n = 3)		
	H#	V	C_M
$\hat{x}$	−0.18	0.14	0.69
$\hat{y}$	0.42	0.53	0.69
$\hat{z}$	−0.01	−0.35	**−0.80**[a]
H_{RGB}	*0.56*[b]	0.41	−0.05
I_{RGB}	0.30	**0.72**[a]	0.36
S_{RGB}	0.12	0.57	**0.74**[a]
Co	−0.06	−0.47	**−0.80**[a]
Cg	−0.20	−0.62	−0.30
Ym	0.36	0.68	0.21

Note. All correlations with $|\rho| \geq 0.21$ are significant at $p < 0.001$.
[a] Boldface indicates $|\rho| \geq 0.70$.
[b] Italics indicate $|\rho| \geq 0.50$ (only highlighted for MSCC H#).

In summary, three MCS-NCS variable pairs were ultimately chosen to allow MSCC measurements to be complemented with the NCS: H# and H_{RGB} ($\rho = 0.56$); V and L ($\rho = 0.73$); and C_M and $\hat{z}$ ($\rho = -0.80$) ($p < 0.001$).

3.5. Quantification of relationships between MSCC and NCS

Regression analysis indicated that variable pairs H# and H_{RGB}, V and L, and C_M and $\hat{z}$ can be defined through linear relationships in which 26% of variation in H# can be explained by H_{RGB} calculations; 54% of variation in V can be explained by L measurements; and 62% of variation in C_M can be explained by $\hat{z}$ calculations (Fig. 3; $p < 0.01$ *for all*). The regression between H# and H_{RGB} is weak; residuals are not randomly distributed, and a pattern is evident where low H# values (H# ≤ 5) have the largest residuals and tend to share a distinct relationship with H_{RGB} when compared to the pattern for H# ≥ 5 (Fig. 3). When separated by physiographic region, regression results between H_{RGB} and H# did not improve ($r^2 = 0.07$ for Coastal Plain sites, $p > 0.01$; $r^2 = 0.33$ for Piedmont sites, $p < 0.01$). The regression between V and L indicates a moderately strong linear relationship with more pronounced scatter for more frequently observed values like 3 through 5, but the model tended to overestimate V for low (<3) values, and underestimate V for high (>6) values. Finally, the regression model for C_M versus $\hat{z}$ highlights a moderately strong negative linear relationship. Residuals are generally negative for $C_M < 3$ and positive for $C_M \geq 4$; in particular, the model underestimates observed C_M for all observations above $C_M = 4$.

In summary, H# and H_{RGB} ranged from 2.5 to 15 and −3.5 to 3.25, respectively, with medians of 7.5 (7.5YR) for H# and −0.25 for H_{RGB} (Table 5). Mean H# (8.4YR) falls between 7.5YR and 10YR but is best approximated by the hue page 7.5YR (Table 5). V and L ranged from 2 to 7 (V) and 13.2 to 60.5 (L), with medians of 4 and 36.7, respectively. Finally, C_M and $\hat{z}$ ranged from 0 to 6 and 0.172 to 0.240 with medians of 4 (C_M) and 0.179 ($\hat{z}$).

Table 5 also indicates statistics for colors that aided in identifying hydric soils and those that did not; t-distribution confidence intervals highlight that statistically significant differences in C_M and $\hat{z}$ occurred between colors involved in hydric soil identification and all other colors ($p < 0.05$). However, L did not differ between hydric versus nonhydric groups ($p > 0.05$).

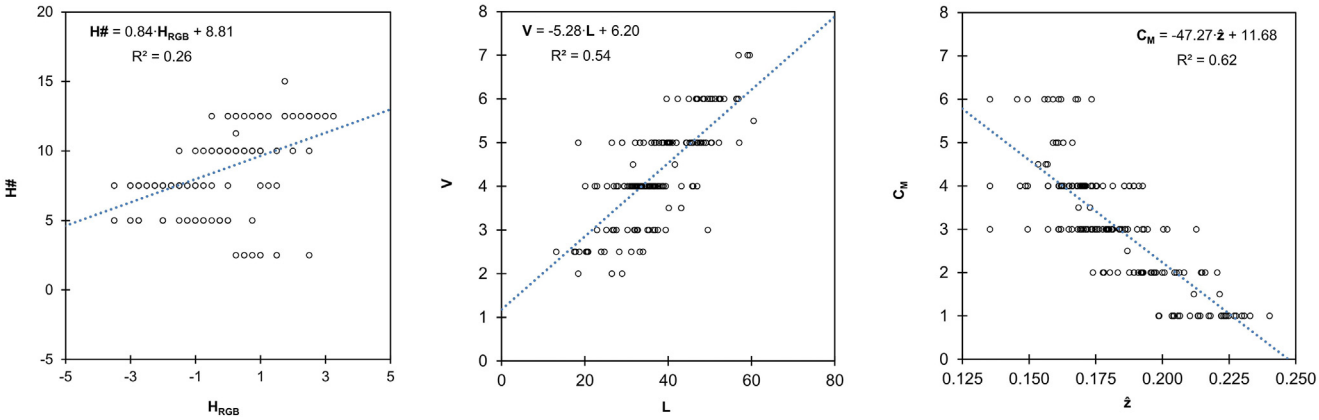

Fig. 3. Scatterplots including regression model trendlines and r^2 coefficients for final NCS-MSCC variable pairs.

4. Discussion

4.1. MSCC and NCS variables

The 15 variables recorded by the NCS provide a broader set of variables and meanings to describe soil color beyond the MSCC. The color spaces supplied through the NCS are not relatable to MSCC variables through well-defined mathematical equations, but certain color spaces have been constructed in such a way—and thoroughly researched with respect to the MSCC—to render them relevant to our study's objective. For example, Lab and LCh were specifically created to relate to human perception of color (e.g., hue, lightness or tone, and chroma or saturation) similar to the MSCC; additionally, the transformation from MSCC to CIE-XYZ, followed by a transformation to CIE-Lab or CIE-LCh, has been studied extensively, making CIE variables attractive for MSCC color space conversions (Fan et al., 2017; Kirillova et al., 2018; Mahyar et al., 2010; Moonrungsee et al., 2015; Torrent and Barrón, 1993; Viscarra Rossel et al., 2006, 2008). While RGB and CMYK variables are device-dependent and not directly related to human perception of color qualities like the MSCC, they have been the focus of previous soils research (Gómez-Robledo et al., 2013; Moonrungsee et al., 2015; Stiglitz et al., 2016a), and their inclusion in our statistical analysis improved chances of identifying strong inter-space correlations. Because each NCS instrument is calibrated before consumer use with guaranteed high inter-instrument agreement, the device dependence of H_{RGB}, selected as the variable most representative of hue, was not deemed an issue for this study. Furthermore, CMYK was chosen as the color space for analysis in a previous study relating the NCS to MSCC soil color measurements, giving precedence to the suitability of such spaces in soil science (Stiglitz et al., 2016a).

4.2. Correlation between soil color variables

The correlation analysis produced promising albeit not affirmative correlations between the NCS and MSCC methods of soil color determination. Intuitively understood NCS variables—for example, L, C, and h—proved most useful for relating NCS colors to MSCC value, but not chroma or hue (Table 3). While V was best correlated with L, C_M was more strongly correlated with calculated variables like $\hat{z}$ than with measured chroma-related variables like C.

The correlation results were not optimal for several reasons. First, the relatively weak correlation coefficients between all NCS variables and MSCC variables—in particular, H#—were unexpected. Research has identified that the mathematical relationship between H and h is more complex than would be expected from their shared meaning (Simon and Frost, 1987). Beyond differences associated with complex color theory, this relatively weak result may be attributable to the relatively low number of MSCC hue pages (and thus values for H#). The introduction of multiple subdivisions between hue pages within the MSCC could provide a higher correlation between MSCC and NCS hue determinations, but would not aid in allowing the NCS to complement conventional color descriptions. Incorporating more complicated calculations such as a redness index, which includes a quotient with cubed variables, may have allowed nonredundant relationships to surface and subsequently may have augmented correlation strengths with h, but would also hinder the goal of this study to find accessible and relatively simple NCS variables to use as proxies for MSCC variables (Kirillova et al., 2015; Sánchez-Marañón et al., 2011; Viscarra Rossel et al., 2006).

A one-to-one transformation between NCS and MSCC color measurements was not achievable from this sample data, but the strong correlation between C_M and $\hat{z}$ highlights a utility of the XYZ color space for relating NCS measurements to the MSCC. It was expected that L and V would have a strong correlation closer to 0.90, demonstrated in past laboratory studies ($r > 0.90$) (Viscarra Rossel et al., 2006); however, the field focus in this study greatly affected the potential to obtain such high correlations. In relating observed MSCC colors to recorded NCS colors, Stiglitz et al. (2016a) found "moderately strong" correlations between MSCC and M_K, Y_K, and K_K of the CMYK color space, where correlation coefficients were 0.51, 0.59, and 0.58 in moist soils, respectively. Our study thus contributes to the literature finding that, while MSCC and NCS colors may be moderately strongly correlated, there exists a high degree of variation among MSCC observations in the field that cannot be explained by NCS measurements. Stiglitz et al. (2016a) converted Munsell readings to CMYK; therefore, it is not possible to tell if the variance for each MSCC reading for V and C mirrored that found in this study. Another study used a model to predict MSCC observations from NCS measurements and found that predictions differed by 0.5 to 3 units in V and 0 to 3 units in C_M (Mancini et al., 2020). Most relevant to using the NCS for hydric soil identification, Mancini et al. (2020) observed that low-chroma colors identified using the MSCC were correctly estimated by the NCS. Their results generally show potential for using the NCS for color measurements when a model has first been calibrated and validated in relating NCS to MSCC. Thus, simple measurements of soil color using both the NCS and MSCC would benefit from models that are calibrated using NCS measurements of MSCC chips.

Within our study, deviations from strong correlations ($|\rho| \geq 0.80$) may be explained by an inability to control for surface texture and soil moisture in the field. These are variables that are always controlled under laboratory settings when high correlations have been determined between MSCC readings and other device readings, and a history of strong evidence exists that indicates they influence both perceived and objective soil color determinations (Fan et al., 2017; Malone et al., 2018; Moonrungsee et al., 2015; Torrent and Barrón, 1993).

Table 5
Summary statistics for final variables of the Munsell Soil Color Chart (MSCC) and Nix Color Sensor (NCS) for wetland soil color reading.

Soil color attribute	Munsell variable		(Min., max.)	Median	Mean ± SE	95% confidence interval	ρ/R^2	NCS variable	(Min., max.)	Median	Mean ± SE	95% confidence interval
Hue[a]	H#		(2.5, 15) ≡ (2.5YR, 5Y)	7.5 (7.5YR)	8.4 ± 0.2 (7.5YR)[b]	(7.8, 8.8) ≡ (7.8YR, 8.8YR)	0.56 0.26	H_{RGB}	(−3.5, 3.25)	−0.25	−0.50 ± 0.12	(−0.73, −0.27)
Value	V		(2, 7)	4	4.3 ± 0.1	(4.2, 4.5)	0.73 0.54	L	(13.2, 60.5)	36.7	37.6 ± 9.5	(36.1, 38.9)
Chroma	C_M		(1, 6)	3	3.1 ± 0.1	(2.8, 3.4)	−0.80 0.62	$\hat{z}$	(0.135, 0.240)	0.178	0.181 ± 0.001	(0.177, 0.185)
Soil colors used in identifying hydric soils	Nonhydric	V	(2, 7)	4	4.1 ± 1.1	(4.0, 4.3)		L	(13.2, 60.5)	36.7	37.6 ± 0.8	(36.1, 39.1)
	Hydric		(4, 6)	5	4.6 ± 0.9	(4.4, 4.8)			(27.5, 52.8)	36.7	39.4 ± 1.0	(37.4, 41.4)
	Nonhydric	C_M*	(1, 6)	4	3.3 ± 1.2	(3.1, 3.5)		$\hat{z}$*	(0.135, 0.231)	0.171	0.174 ± 0.001	(0.171, 0.176)
	Hydric		(1, 2)	1	1.3 ± 0.5	(1.1, 1.4)			(0.172, 0.240)	0.202	0.204 ± 0.002	(0.200, 0.209)

[a] Represented as both H# and Munsell H.
[b] Mean H# of 8.4 is the most comparable to the MSCC hue page 7.5YR.
* $p < 0.05$ for the 2-sample t-test.

Nonetheless, these are properties of soil that cannot always be controlled in the field; one recommendation for future studies using the NCS in the field would be to moisten soils enough to be able to form a flat smooth surface upon which the NCS can be placed when doing color measurements and avoiding soil saturated beyond a certain extent. However, as soil colors can become homogenized when rubbed, such a protocol may risk a loss of in-situ soil colors. Because high soil moisture is likely to be encountered when investigating wetland soil colors, further study is necessary to quantify the relationship between the hydrologic conditions of sites and their soil colors to build a much stronger and universal relationship for many different types of soils over a large geographic extent.

4.3. Relationships between NCS and MSCC variables

Overall, the high collinearity identified within each method makes a strong case for relying on univariate regression instead of using a multidimensional approach that requires multiple NCS variables to explain each MSCC variable. Nonetheless, while the regression analysis highlights that V and C_M can be explained by NCS variables to a modest degree identified as adequate by this study's standards ($r^2 \geq 0.50$), large spread and nonrandom residuals indicate that MSCC readings may not be dependably estimated from NCS variables using our regression models (Fig. 3).

Particularly for the weak H#-H_{RGB} regression model ($r^2 = 0.26$), large ranges in NCS measurements for a given discrete MSCC measurement (e.g., $H_{RGB} = 0.5$) suggest inadequate control over sources of error using the NCS. Controlling for physiographic region reduced predictive power of the regression models, with high standard errors in NCS measurements for each discrete H# despite similar ranges (see Section 3.5); this indicates that measuring soils with similar texture characteristics may not be sufficient to reduce error. Instead, increasing the predictive power of MSCC-NCS regression models should focus on the standardization of methods after sampling soils and before measuring color—e.g., controlling for soil moisture, surface roughness, lighting conditions when using the MSCC.

Stiglitz et al. (2016a) highlighted the strong capacity for the NCS to detect color changes due to moisture, which suggests that the NCS measurements may be more sensitive than human-dependent MSCC judgments concerning color changes due to moisture. Furthermore, light scattering is known to depend on surface roughness or evenness, and this relationship can extend to micro-scale roughness within the NCS aperture that affects color determinations (Wu et al., 2009). Finally, while standard operating procedures for MSCC use advise users to take measures to limit misinterpretations due to lighting conditions, field operations—particularly in forested wetlands—are not necessarily able to work around time of day or micro-habitat lighting conditions that are affected by canopy cover and may affect MSCC judgments (Turk and Young, 2020). While lab-based studies can better control moisture content, surface evenness, and lighting-dependent judgments of soil color, steps can nonetheless be taken in the field to minimize the error due to these issues. For example, higher priority should be placed on creating a smooth surface for each soil ped using a knife while minimizing the mixing of colors present on the soil surface. Additionally, when using both methods of color determination, taking NCS measurements before MSCC measurements, or ensuring that each soil ped is rewetted before utilizing the opposing method, may reduce changes in soil moisture that affect objective and perceived soil color. Further study should specifically focus on how to control these issues without manipulating in-situ soil colors through reducing roughness and without overcomplicating the efficiency that the NCS can offer in the process.

Regression models between MSCC variables and H_{RGB}, L, and $\hat{z}$ may also improve through increasing the sample size and diversity of measured colors, as the observations of this study were comprised of only 53 unique combinations of (H, V, C_M) common to the Virginia Piedmont and Coastal Plain. For example, very few soils with colors redder than

5YR were identified at our field sites. If the medians of H_{RGB} are examined for each discrete H# in Fig. 3, it appears that the more commonly observed colors—i.e., H# = 5 (5YR), 7.5 (7.5YR), 10 (10YR), and 12.5 (2.5Y) – follow a slightly different trend with a steeper slope than identified using the regression equation; this is the result of H_{RGB} values for H# = 2.5 (H = 2.5YR) plotting considerably higher than would be expected from the perceivable H#-H_{RGB} relationship for yellower hues (higher H#). More measurements for soils with hues of 2.5YR and redder may be necessary to determine if our data accurately depict an inability for the NCS to follow a predictable trend in soil redness past a certain threshold.

The scatterplots of Fig. 3 also indicate large spread and nonrandom residuals for the C_M-$\hat{z}$ model despite the pair's high correlation coefficient. For $C_M = 1$, outliers appear to be decreasing the explanatory power of the line of best fit; for $C_M > 5$, the onset of a nonlinear trend produces systematically positive residuals (Fig. 3). The results of the regression may be improved by creating a regression modeled from the median and interquartile range associated with each discrete chroma rather than using the entire dataset; for example, obtaining $\hat{z} < 0.175$ would be indicative of $C_M > 2$ with a higher degree of certainty. The nonlinear relationship for $C_M > 5$ may suggest a nonlinear relationship even with improved quality control and method standardization, warranting further study.

Overall, the discrete nature of H#, V, and C_M complicate regression interpretation even with normal residuals: MSCC versus NCS scatterplots are unlikely to be either onto or one-to-one, with a spectrum of NCS variable measurements mapped to a single MSCC variable measurement, and multiple MSCC measurements mapped to a single NCS variable measurement. Therefore, using the NCS as a color determination tool is more likely to provide range estimates of MSCC variables instead of point estimates. However, point estimates can still be useful and can be improved through regression analyses with reduced variances and randomly distributed residuals.

4.4. Utility of methodology for soil science and education

Our analysis does not support the notion that the NCS can be depended upon by professionals to identify soil colors, including wetland soil colors, without greater method standardization and quality control. An important aspect of color determination in assisting hydric field indicators is the capacity to discriminate between chromas of 2 or less and chromas greater than 2, but large overlap occurred for $\hat{z}$ between these two sets such that professionals characterizing soil color would not be able to discern the hydric nature of a soil if $\hat{z}$ fell within this range of overlap (e.g., 0.175 to 0.225).

Nonetheless, the methodology of identifying relationships between NCS and MSCC variables was able to identify moderately strong to strong correlations that suggest a focus on characterizing NCS variables is relevant to its application to soil science and education. Certain NCS measured and calculated variables can be linked to the aspects of color from the MSCC—hue, value, and chroma—in a generalized way through identifying trends in increasing/decreasing NCS variables as a signal of higher or lower numbers for MSCC variables, or extrema in NCS variable ranges highlighting extrema in MSCC variable ranges. For example, citizen science education endeavors using the NCS in Northern Virginia could highlight the high probability that colors do not meet the hydric soil thresholds for depletions if L and $\hat{z}$ do not fall within the hydric ranges of Table 5. Such an approach would augment the shortcomings of using the MSCC—requiring familiarity for proper judgment, influenced by sunlight and moisture, and requiring sometimes time-consuming judgments—and provide an accessible, relatively fast method of exploring soil colors.

Furthermore, the NCS has the capacity to be used cautiously in assisting MSCC measurements and identifying hydric soils in less technical and more education-focused endeavors when users are more familiar with alternative color spaces like CIE-Lab, RGB, or CMYK. While variables like H_{RGB} and $\hat{z}$ may be unfamiliar to users, their introduction into soil science and education could yield a new pathway of characterizing and parametrizing soil colors that ultimately appear less like algebraic calculations and more like intuitive indicators of color. With future efforts focused on improving the breadth of colors measured using both measurement devices and removing sources of error by working to standardize surface texture, moisture, and other confounding variables met during field work, the shortcomings highlighted in this study can be addressed with promising applications.

5. Conclusions

This study shows that NCS variables can be characterized and quantitatively related to MSCC variables to a modest or strong degree. The correlation and regression analyses of the two field methods for soil color measurement indicate that MSCC H, V, and C_M variables of soil colors, commonly observed and reported for wetland delineation, can be represented from modest (H), moderately strong (V), and strong (C_M) relationships with NCS variables H_{RGB}, L, and $\hat{z}$, respectively. With over 35% of variation in each MSCC variable left unexplained by matching NCS variables, field use of the NCS by professionals cannot yet be supported using the methods of this study; nonetheless, correlations between MSCC V and C_M and NCS variables indicate a promising role of the NCS in characterizing soil colors with further refinement following similar calculations and statistical analyses presented herein. More fine-tuning is necessary to properly harness what the NCS can offer, and future endeavors should determine if a standardization of field methods can render the NCS able to measure color accurately and reliably as related to MSCC measurements.

CRediT authorship contribution statement

Stephanie Schmidt: Data Collection (Field work), Data Analysis, Writing-Original draft preparation.

Changwoo Ahn: Conceptualization, Supervision, Data Analysis, Writing-Reviewing and Editing.

Declaration of competing interest

The authors declare that they have no known competing financial interests or personal relationships that could have appeared to influence the work reported in this paper.

Acknowledgments

This study was largely internally driven but required support from several field volunteers including Katie Ledford, Jesse Wong, and other students from Dr. Ahn's undergraduate classes from 2018 to 2019.

Funding

This research did not receive any specific grant from funding agencies in the public, commercial, or not-for-profit sectors.

References

Ahn, C., Gillevet, P.M., Sikaroodi, M., Wolf, K.L., 2009. An assessment of soil bacterial community structure and physicochemistry in two microtopographic locations of a palustrine forested wetland. Wetl. Ecol. Manag. 17 (4), 397–407. https://doi.org/10.1007/s11273-008-9116-4.

Aitkenhead, M., Donnelly, D., Coull, M., Gwatkin, R., 2016. Estimating soil properties with a mobile phone. In: Hartemink, A.E., Minasny, B. (Eds.), Digital Soil Morphometrics. Springer International Publishing, pp. 89–110 https://doi.org/10.1007/978-3-319-28295-4_7.

Akoglu, H., 2018. User's guide to correlation coefficients. Turk. J. Emerg. Med. 18 (3), 91–93. https://doi.org/10.1016/j.tjem.(2018).08.001.

Al-rasheed, A.S., 2015. Categorical perception of color: evidence from secondary category boundary. Psychol. Res. Behav. Manag. 8, 273. https://doi.org/10.2147/PRBM.S78348.

Campos, R.C., Demattê, J.A.M., 2004. Soil color: approach to a conventional assessment method in comparison to an automatization process for soil classification. Rev. Bras. Cienc. Solo 28 (5), 853–863. https://doi.org/10.1590/S0100-06832004000500008.
Dancey, C.P., Reidy, J., 2007. Statistics Without Maths for Psychology. Pearson Education, New York, NY.
Environmental Laboratory, 1987. Corps of Engineers Wetland Delineation Manual. United States Army Corps of Engineers https://www.lrh.usace.army.mil/Portals/38/docs/USACE%2087%20Wetland%20Delineation%20Manual.pdf [16 July 2020].
Evans, C.V., Franzmeier, D.P., 1988. Color index values to represent wetness and aeration in some Indiana soils. Geoderma 41 (3–4), 353–368. https://doi.org/10.1016/0016-7061(88)90070-5.
Fairchild, M.D., 2013. Color Appearance Models. John Wiley & Sons, Chichester, West Sussex, United Kingdom.
Fan, Z., Herrick, J.E., Saltzman, R., Matteis, C., Yudina, A., Nocella, N., Crawford, E., Parker, R., Van Zee, J., 2017. Measurement of soil color: a comparison between smartphone camera and the Munsell Color Charts. Soil Sci. Soc. Am. J. 81 (5), 1139–1146. https://doi.org/10.2136/sssaj2017.01.0009.
Federal Register, 1994. Changes in hydric soils of the United States. https://www.gpo.gov/fdsys/pkg/FR-1994-07-13/html/94-16835.htm [16 July 2020].
Fuller, B.G., 2007. Banshee Reeks Nature Preserve general management plan. Loudoun County Department of Parks, Recreation, and Community Services – Division of Facilities Planning and Development.
Genthner, M.H., Daniels, W., Hodges, R.L., Thomas, P., 1998. Redoximorphic features and seasonal water table relations, Upper Coastal Plain, Virginia. In: Rabenhorst, M.C., McDaniel, P.A. (Eds.), Quantifying Soil Hydromorphology. vol. 54. Soil Science Society of America, Madison, WI, pp. 43–60. https://doi.org/10.2136/sssaspecpub54.c3.
Gómez-Robledo, L., López-Ruiz, N., Melgosa, M., Palma, A.J., Capitán-Vallvey, L.F., Sánchez-Marañón, M., 2013. Using the mobile phone as Munsell soil-colour sensor: an experiment under controlled illumination conditions. Comput. Electron. Agric. 99, 200–208. https://doi.org/10.1016/j.compag.2013.10.002.
Guertal, W.R., Hall, G.F., 1990. Relating soil color to water table levels. Ohio J. Sci. 90 (44), 118–124.
Gupta, R.K., Abrol, I.P., Finkl, C.W., Kirkham, M.B., Arbestain, M.C., Macías, F., Chesworth, W., Germida, J.J., Loeppert, R.H., Cook, M.G., 2008. Soil color. In: Chesworth, W. (Ed.), Encyclopedia of Soil Science. Springer, Dordrecht, The Netherlands, pp. 641–643 https://doi.org/10.1007/978-1-4020-3995-9_534.
Han, P., Dong, D., Zhao, X., Jiao, L., Lang, Y., 2016. A smartphone-based soil color sensor: for soil type classification. Comput. Electron. Agric. 123, 232–241. https://doi.org/10.1016/j.compag.2016.02.024.
He, X., Vepraskas, M., Lindbo, D., Skaggs, R., 2003. A method to predict soil saturation frequency and duration from soil color. Soil Sci. Soc. Am. J. 67 (3), 961–969. https://doi.org/10.2136/sssaj2003.9610.
Ibáñez-Asensio, S., Marqués-Mateu, Á., Moreno-Ramón, H., Balasch, S., 2013. Statistical relationships between soil colour and soil attributes in semiarid areas. Biosyst. Eng. 116 (2), 120–129. https://doi.org/10.1016/j.biosystemseng.2013.07.013.
Jien, S., Hseu, Z., Chen, Z., 2004. Relations between morphological color index and soil wetness condition of anthraquic soils in Taiwan. Soil Sci. 169 (12), 871–882. https://doi.org/10.1097/01.ss.0000149364.73688.68.
Jones, E.J., McBratney, A.B., 2016. In situ analysis of soil mineral composition through conjoint use of visible, near-infrared and X-ray fluorescence spectroscopy. Digital Soil Morphometrics. Springer, pp. 51–62.
Kellogg, C.E., 1937. Soil Survey Manual. USDA, Miscellaneous Publication No. 274. https://www.nrcs.usda.gov/Internet/FSE_documents/nrcseprd1335010.pdf [8 March 2021].
Ketterings, Q.M., Bigham, J.M., 2000. Soil color as an indicator of slash-and-burn fire severity and soil fertility in Sumatra, Indonesia. Soil Sci. Soc. Am. J. 64 (5), 1826–1833. https://doi.org/10.2136/sssaj2000.6451826x.
Kirillova, N., Vodyanitskii, Y.N., Sileva, T., 2015. Conversion of soil color parameters from the Munsell system to the CIE-L* a* b* system. Eurasian Soil Sci. 48 (5), 468–475. https://doi.org/10.1134/S1064229315050026.
Kirillova, N.P., Grauer-Gray, J., Hartemink, A.E., Sileova, T.M., Artemyeva, Z.S., Burova, E.K., 2018. New perspectives to use Munsell color charts with electronic devices. Comput. Electron. Agric. 155, 378–385. https://doi.org/10.1016/j.compag.2018.10.028.
Mahyar, F., Cheung, V., Westland, S., 2010. Different transformation methods between CIELAB coordinates and Munsell hue. Color. Technol. 126 (1), 31–36. https://doi.org/10.1111/j.1478-4408.2010.00224.x.
Malone, B.P., McBratney, A.B., Minasny, B., 2018. Description and spatial inference of soil drainage using matrix soil colours in the Lower Hunter Valley, New South Wales, Australia. PeerJ. 6, e4659. https://doi.org/10.7717/peerj.4659.
Malvar, H.S., Sullivan, G.J., Srinivasan, S., 2008. Lifting-based reversible color transformations for image compression. Applications of Digital Image Processing XXXI. vol. 7073. International Society for Optics and Photonics, p. 707307. https://doi.org/10.1117/12.797091.
Mancini, M., Weindorf, D.C., Monteiro, M.E.C., de Faria, Á.J.G., dos Santos Teixeira, A.F., de Lima, W., de Lima, F.R.D., Dijair, T.S.B., Marques, F.D., Ribeiro, D., Silva, S.H.G., Chakraborty, S., Curi, N., 2020. From sensor data to Munsell color system: machine learning algorithm applied to tropical soil color classification via NixTM Pro sensor. Geoderma 375, 114471. https://doi.org/10.1016/j.geoderma.
Marqués-Mateu, Á., Balaguer-Puig, M., Moreno-Ramón, H., Ibáñez-Asensio, S., 2015. A laboratory procedure for measuring and georeferencing soil colour. Int. Arch. Photogramm. Remote. Sens. Spat. Inf. Sci. Gottingen 40 (7), 57–64. https://doi.org/10.5194/isprsarchives-XL-7-W3-57-2015.
Menne, M.J., Durre, I., Korzeniewski, B., McNeal, S., Thomas, K., Yin, X., Anthony, X., Ray, R., Vose, R.S., Gleason, B.E., Houston, T.G., 2012. Global Historical Climatology Network - Daily (GHCN-Daily), Version 3. [Daily Summaries]. NOAA National Climatic Data Center https://doi.org/10.7289/V5D21VHZ [11 July 2020].
Moonrungsee, N., Pencharee, S., Jakmunee, J., 2015. Colorimetric analyzer based on mobile phone camera for determination of available phosphorus in soil. Talanta 136, 204–209. https://doi.org/10.1016/j.talanta.2015.01.024.
Moritsuka, N., Matsuoka, K., Katsura, K., Sano, S., Yanai, J., 2014. Soil color analysis for statistically estimating total carbon, total nitrogen and active iron contents in Japanese agricultural soils. Soil Sci. Plant Nutr. 60 (4), 475–485. https://doi.org/10.1080/00380768.2014.906295.
Mukaka, M.M., 2012. Statistics corner: a guide to appropriate use of correlation coefficient in medical research. Malawi Med. J. 24 (3), 69–71.
Munsell, A.H., 1905. A Color Notation. G. H. Ellis Company, Boston, MA.
Munsell Color, 2009. Munsell Soil Color Chart. X-Rite.
O'Donnell, T.K., Goyne, K.W., Miles, R.J., Baffaut, C., Anderson, S.H., Sudduth, K.A., 2010. Identification and quantification of soil redoximorphic features by digital image processing. Geoderma 157 (3–4), 86–96. https://doi.org/10.1016/j.geoderma.2010.03.019.
O'Donnell, T.K., Goyne, K.W., Miles, R.J., Baffaut, C., Anderson, S.H., Sudduth, K.A., 2011. Determination of representative elementary areas for soil redoximorphic features identified by digital image processing. Geoderma 161 (3–4), 138–146. https://doi.org/10.1016/j.geoderma.2010.12.011.
Paul, J., 2017, March 24. In our backyard: Banshee Reeks, a Virginia treasure. Loudoun Now http://loudounnow.com/2017/03/24/in-our-backyard-banshee-reeks-a-virginia-treasure/ [30 April 2020].
Pretorius, M., Huyssteen, C., Brown, L., 2017. Soil color indicates carbon and wetlands: developing a color-proxy for soil organic carbon and wetland boundaries on sandy coastal plains in South Africa. Environ. Monit. Assess. 189 (11), 1–18. https://doi.org/10.1007/s10661-017-6249-z.
Rabenhorst, M., Schmehling, A., Thompson, J.A., Hirmas, D.R., Graham, R.C., Rossi, A.M., 2015. Reliability of soil color standards. Soil Sci. Soc. Am. J. 79 (1), 193–199. https://doi.org/10.2136/sssaj2014.10.0401.
Richardson, J., Hole, F., 1979. Mottling and iron distribution in a Glossoboralf-Haplaquoll hydrosequence on a glacial moraine in Northwestern Wisconsin. Soil Sci. Soc. Am. J. 43 (3), 552–558. https://doi.org/10.2136/sssaj1979.03615995004300030024x.
Ruck, L., Brown, C.T., 2015. Quantitative analysis of Munsell color data from archeological ceramics. J. Archaeol. Sci. Rep. 3, 549–557. https://doi.org/10.1016/j.jasrep.2015.08.014.
Sánchez-Marañón, M., 2011. Color indices, relationship with soil characteristics. In: Gliński, J., Horabik, J., Lipiec, J. (Eds.), Encyclopedia of Agrophysics. Springer, Dordrecht, The Netherlands, pp. 141–145 https://doi.org/10.1007/978-90-481-3585-1_237.
Sánchez-Marañón, M., García, P.A., Huertas, R., Hernández-Andrés, J., Melgosa, M., 2011. Influence of natural daylight on soil color description: assessment using a color-appearance model. Soil Sci. Soc. Am. J. 75 (3), 984–993. https://doi.org/10.2136/sssaj2010.0336.
Sanyal, S., Amrani, F., Dallongeville, A., Banerjee, S., Blanchard, O., Deguen, S., et al., 2017. Estimating indoor galaxolide concentrations using predictive models based on objective assessments and data about dwelling characteristics. Inhal. Toxicol. 29 (12–14), 611–619. https://doi.org/10.1080/08958378.2018.1432729.
Schmidt, S.A., Ahn, C., 2019. A comparative review of methods of using soil colors and their patterns for wetland ecology and management. Commun. Soil Sci. Plant Anal. 50 (11), 1293–1309. https://doi.org/10.1080/00103624.2019.1604737.
Schober, P., Boer, C., Schwarte, L., 2018. Correlation coefficients: Appropriate use and interpretation. Anesth. Analg. 126 (5), 1763–1768. https://doi.org/10.1213/ANE.0000000000002864.
Schwertmann, U., 1993. Relations between iron oxides, soil color, and soil formation. In: Bigham, J.M., Ciolkosz, E.J. (Eds.), Soil Color. vol. 31, pp. 51–69. https://doi.org/10.2136/sssaspecpub31.c4.
Schwertmann, U., Lentze, W., 1966. Soil color and iron oxide forms. Z. Pflanzenernaehr. Düngung Bodenkd. 115 (3), 209–214. https://doi.org/10.1002/jpln.19661150307.
Shields, J.A., St. Arnaud, R.J., Paul, E.A., Clayton, J.S., 1966. Measurement of soil color. Can. J. Soil Sci. 46 (1), 83–90. https://doi.org/10.4141/cjss66-012.
Simon, F.T., Frost, J.A., 1987. A new method for the conversion of CIE colorimetric data to Munsell notations. Color. Res. Appl. 12 (5), 256–260. https://doi.org/10.1002/col.5080120506.
Simonson, G.H., Boersma, L., 1972. Soil morphology and water table relations: II. Correlation between annual water table fluctuations and profile features. Soil Sci. Soc. Am. J. 36 (4), 649–653. https://doi.org/10.2136/sssaj1972.03615995003600040041x.
Simonson, R.W., 1989. Historical highlights of soil survey and soil classification with emphasis on the United States, 1899–1970. Technical Paper No. 18. International Soil Reference and Information Centre (ISRIC) , p. 86. https://www.isric.org/index.php/documents/document-type/technical-paper-18-historical-highlights-soil-survey-and-soil [15 July 2020].
Simonson, R.W., 1993. Soil color standards and terms for field use—history of their development. In: Bigham, J.M., Ciolkosz, E.J. (Eds.), Soil Color. vol. 31, pp. 1–20. https://doi.org/10.2136/sssaspecpub31.c1.
Stiglitz, R., Mikhailova, E., Post, C., Schlautman, M., Sharp, J., 2016a. Evaluation of an inexpensive sensor to measure soil color. Comput. Electron. Agric. 121, 141–148. https://doi.org/10.1016/j.compag.2015.11.014.
Stiglitz, R., Mikhailova, E., Post, C., Schlautman, M., Sharp, J., 2016b. Teaching soil color determination using an inexpensive color sensor. Nat. Sci. Educ. 45 (1). https://doi.org/10.4195/nse2016.03.0005.
Stiglitz, R., Mikhailova, E., Post, C., Schlautman, M., Sharp, J., 2017a. Using an inexpensive color sensor for rapid assessment of soil organic carbon. Geoderma 286, 98–103. https://doi.org/10.1016/j.geoderma.2016.10.027.
Stiglitz, R., Mikhailova, E., Post, C., Schlautman, M., Sharp, J., Pargas, R., Glover, B., Mooney, J., 2017b. Soil color sensor data collection using a GPS-enabled smartphone application. Geoderma 296, 108–114. https://doi.org/10.1016/j.geoderma.2017.02.018.

Summers, D., Lewis, M., Ostendorf, B., Chittleborough, D., 2011. Visible near-infrared reflectance spectroscopy as a predictive indicator of soil properties. Ecol. Indic. 11 (1), 123–131. https://doi.org/10.1016/j.ecolind.2009.05.001.

Thompson, J.A., Bell, J.C., 1996. Color index for identifying hydric conditions for seasonally saturated Mollisols in Minnesota. Soil Sci. Soc. Am. J. 60 (6), 1979. https://doi.org/10.2136/sssaj1996.03615995006000060051x.

Tiner, R.W., 2017. Wetland Indicators: A Guide to Wetland Identification, Delineation, Classification, and Mapping. 2nd. CRC Press, Boca Raton, FL http://www.ncwetlands.org/wp-content/uploads/Tiner-2017-Wetland-indicators.pdf [10 July 2020].

Torrent, J., Barrón, V., 1993. Laboratory measurement of soil color: theory and practice. Soil Color, 21–33 https://doi.org/10.2136/sssaspecpub31.c2.

Turk, J.K., Young, R.A., 2020. Field conditions and the accuracy of visually determined Munsell soil color. Soil Sci. Soc. Am. J. 84 (1), 163–169. https://doi.org/10.1002/saj2.20023.

US Fish and Wildlife Service, 2010. Elizabeth Hartwell Mason Neck and Featherstone National Wildlife Refuges: Draft Comprehensive Conservation Plan and the Environmental Assessment. United States Department of the Interior https://www.fws.gov/northeast/planning/MasonNeck_Featherstone/draftccp/Entire_Document.pdf [15 November 2018].

USDA–NRCS Soil Survey Staff, 2020a. Web Soil Survey, Version 3.4.0. Fairfax County, VA, USA. http://websoilsurvey.nrcs.usda.gov/app/WebSoilSurvey.aspx?aoissa=VA600 [2 July 2020].

USDA–NRCS Soil Survey Staff, 2020b. Web Soil Survey, Version 3.4.0. Loudoun County, VA, USA. http://websoilsurvey.nrcs.usda.gov/app/WebSoilSurvey.aspx?aoissa=VA107 [2 July 2020].

USDA–NRCS Soil Survey Staff, 2020c. Web Soil Survey, Version 3.4.0. Prince William County, VA, USA. http://websoilsurvey.nrcs.usda.gov/app/WebSoilSurvey.aspx?aoissa=VA153 [2 July 2020].

Field indicators of hydric soils in the United States (version 8.2). In: Vasilas, L.M., Hurt, G.W., Berkowitz, J.F. (Eds.), USDA–NRCS, in Cooperation With the National Technical Committee for Hydric Soils https://www.nrcs.usda.gov/Internet/FSE_documents/nrcs142p2_053171.pdf [12 July 2020].

Vepraskas, M.J., 2015. Redoximorphic features for identifying aquic conditions. Technical Bulletin No. 301. North Carolina Agricultural Research Service, NC State University, Raleigh, North Carolina https://content.ces.ncsu.edu/redoximorphic-features-for-identifying-aquic-conditions.pdf [17 July 2020].

Vepraskas, M.J., Craft, C.B., 2016. Wetland Soils: Genesis, Hydrology, Landscapes, and Classification. 2nd. CRC Press, Boca Raton, FL.

Vepraskas, M.J., Lindbo, D.L., 2012. Redoximorphic features as related to soil hydrology and hydric soils. Hydropedology. Elsevier, pp. 143–172 https://doi.org/10.1016/B978-0-12-386941-8.00005-8.

Vepraskas, M.J., He, X., Lindbo, D.L., Skaggs, R.W., 2004. Calibrating hydric soil field indicators to long-term wetland hydrology. Soil Sci. Soc. Am. J. 68 (4), 1461–1469. https://doi.org/10.2136/sssaj2004.1461.

Viscarra Rossel, R.A., Minasny, B., Roudier, P., McBratney, A.B., 2006. Colour space models for soil science. Geoderma 133 (3), 320–337. https://doi.org/10.1016/j.geoderma.2005.07.017.

Viscarra Rossel, R.A., Fouad, Y., Walter, C., 2008. Using a digital camera to measure soil organic carbon and iron contents. Biosyst. Eng. 100 (2), 149–159. https://doi.org/10.1016/j.biosystemseng.2008.02.007.

Viscarra Rossel, R.A., Cattle, S.R., Ortega, A., Fouad, Y., 2009. In situ measurements of soil colour, mineral composition and clay content by vis–NIR spectroscopy. Geoderma 150 (3), 253–266. https://doi.org/10.1016/j.geoderma.2009.01.025.

Wetland Studies and Solutions Inc., 2020. Julie J. Metz Wetland Bank. https://www.wetlands.com/julie-metz [15 November 2020].

Wu, C.-Y., Jacobson, A.R., Laba, M., Baveye, P.C., 2009. Accounting for surface roughness effects in the near-infrared reflectance sensing of soils. Geoderma 152 (1), 171–180. https://doi.org/10.1016/j.geoderma.2009.06.002.

Yang, S., Fang, X., Li, J., An, Z., Chen, S., Hitoshi, F., 2001. Transformation functions of soil color and climate. Sci. China Ser. D Earth Sci. 44 (1), 218–226. https://doi.org/10.1007/BF02911990.